ϵ-greedy automated indentation of cementitious materials for phase mechanical properties determination

Benoit Hilloulin, Mathieu Lagrange, Marius Duvillard, Gauthier Garioud

ε–greedy automated indentation of cementitious materials for phase mechanical properties determination

B. Hilloulin[1], M. Lagrange[2], M. Duvillard[3], G. Garioud[3]

[1] *Institut de Recherche en Génie Civil et Mécanique (GeM), UMR-CNRS 6183, Ecole Centrale de Nantes, 1 rue de la Noë, 44321 Nantes, France – e-mail: benoit.hilloulin@ec-nantes.fr*

[2] *Laboratoire des Sciences du Numérique de Nantes – CNRS, Ecole Centrale de Nantes, 1 rue de la Noë, 44321 Nantes, France – email : mathieu.lagrange@cnrs.f*

[3] *Ecole Centrale de Nantes, 1 rue de la Noë, 44321 Nantes, France*

ABSTRACT

Microindentation and nanoindentation tests are very useful to assess the micromechanical properties of materials. However, statistical indentation tests require large matrices of indents for heterogeneous materials, which can be time-consuming. Given that specific properties of only one phase of interest can be looked for, a novel procedure is proposed to locate indents automatically. The procedure uses an ε–greedy strategy to determine the next indents to perform. The strategy is informed by the nature of predicted indents using unsupervised clustering of the indentation curves and Gaussian Process Classification. The influence of several parameters has been assessed, and the best combination performance has been quantified in the case of the microindentation of a cementitious mortar sample (500 mN) and the nanoindentation of a cement paste (1 mN). The proportion of indents in the phase of interest increased by around 20% in both cases, paving the way for faster indentation experiments.

HIGHLIGHTS

- ε–greedy strategies can automatically locate the next indents to perform in a phase of interest during indentation.
- The technique is used for cementitious materials at the micro- and the nanoscale.
- The proportion of indents in the phase of interest can increase by around 20%.
- Indentation curves are interpreted by unsupervised learning and Gaussian processes.
- The algorithm's parameters can be tuned to increase the global performance.

KEYWORDS

Indentation; Machine Learning; Phase properties; ε–greedy strategy; Material Characterization; Cementitious materials

1. Introduction

Indentation is one of the primary techniques used to assess the mechanical properties of materials at various scales and can typically help design new materials or assess materials' durability against degradation. Microindentation and nanoindentation have been extensively developed during the last decades to measure the elastic [1,2] and viscoelastic properties of material phases [3–5] or hardening properties [6]. Load ranges of around some millinewtons, resp. nanonewtons, employed in microindentation, resp. nanoindentation, typically induce penetration depth of some hundreds of nanometers or micrometers, resp. tens of nanometers, providing information about the local mechanical properties. Hardness, indentation modulus [7], and eventually parameters influencing time-dependent properties such as the creep modulus can be derived based on the indentation measurements [8–11].

The grid indentation technique, consisting of performing a regular grid of hundreds or thousands of indents over of representative area of heterogeneous material, has been employed

to supplement single indentation results [12,13]. Grid indentation measurements usually take some tens of hours under precisely-controlled experimental conditions. Using deconvolutions techniques on the outputs such as least square optimization [14], unsupervised clustering such as k-means [15], hierarchical clustering [16] or Gaussian mixture models [17], the relative proportions of the various phases and their main mechanical properties can be inferred. The phase properties can then help monitor the material evolution during manufacturing or any eventual degradation. The elastic or viscoelastic properties of the phases also help assess the global material properties using analytical or numerical homogenization techniques [18–21] or the full-field measurement approach [22].

Importantly, some phases in heterogeneous materials might need specific attention, as they constitute the most sensitive phase subjected to mechanical properties evolutions and alterations. For example, in cementitious materials such as concrete, the major phases at a pluri-micrometric scale are aggregate, sand and cement paste. Cement paste evolution attracts most of the researchers' attention as it might develop more of less stiffness and strength during hydration, depending on the initial mix or because of the various degradations it might face due to adverse environmental conditions such as leaching [18,23], shrinkage [24], sulfate attack [25,26], chloride ingress [27] or irradiations [28]. At the nanoscale, cement paste comprises several hydrated phases, the major ones being calcium silicate hydrates (C-S-H) gel and portlandite crystals. Depending on the nature of the phenomenon inducing mechanical properties changes, one of the two phases is generally altered first, e.g., portlandite concerning leaching for example, or, for instance, C-S-H during the initial hydration depending on the mix composition and the relative proportion of supplementary cementitious materials used to lower the environmental impact of concrete [29]. For this reason, more precise information about a phase of interest can be required. Additional tests have been coupled with indentation, such as imaging [16,30,31] or chemical analysis [32], both at a microscale [33,34] or a macroscale [35].

Although adding experimental work, these tests provide interesting information that can help refine the deconvolution and allow the identification of a phase of interest more precisely. Besides, Bayesian approaches, based on indentation curves alone, have recently been developed to assess more precisely the mechanical properties of various phases during nanoindentation [36].

To circumvent the drawbacks of grid indentation to assess the properties of one particular phase of interest in a heterogeneous material, the possibility of locating indents in a phase of interest during the indentation process, i.e., online, is investigated herein. Innovative online algorithms and, more particularly, exploration-exploitation strategies are being developed for some years for automating the speeding of specific tasks. Map exploration problems can be tackled without particular initial knowledge, for example, to guide robots exploration effectively [37,38]. Using artificial intelligence techniques and increasing machine knowledge during exploration [39], objectives, such as finding specific objects in a map or exploring this map, can be fulfilled in several environments such as households [40] or industrial sites [41].

In this study, an exploration–exploitation strategy, namely, ε–greedy, has been developed to locate the highest number of indents in a phase of interest during the microindentation or nanoindentation process of typical heterogeneous materials, e.g., mortar and cement paste. According to the strategy, after a rather loose initial grid indentation test, some specific indents were gradually selected among the remaining potential indent locations. To determine those locations, the proposed algorithm is based on an ε–greedy strategy informed by a Gaussian process classification to determine the nature of unknown indents, and unsupervised clustering to separate the performed indents into groups related to the phases in the material. The proposed method is satisfactorily compared to grid indentation performance, e.g., the random selection of the indents.

The article is structured as follows: the first section describes the two materials used in the study, e.g., cementitious mortar and cement paste, and the numerical methods are then explained. Two versions of the algorithm are detailed to decouple the relative influence of the input parameters: one offline algorithm that can regularly check the indents nature based on microscopic information, and one online algorithm only informed by indentation curves. The results are presented in the following section. First, the convergence of the algorithm, the main parameters of the GPC and the ε–greedy strategy are discussed using the 'offline' algorithm. Secondly, the efficiency of the online algorithm that considers only the unsupervised clustering of the indentation curves is then evaluated. Conclusions are finally drawn concerning the interest of these methods, and future research directions are proposed.

2. Materials and methods

2.1 Experimental methods

2.1.1 Preparation of cement paste and mortar samples

Mortar specimens and cement paste specimens were prepared using CEM I 52.5 cement and 0/4 mm calcareous sand. The mortar formulation was determined to be as representative as possible of high-performance concrete. Both formulations are reported in Table 1.

Table 1. Mortar and cement paste compositions (kg / m^3)

Specimen	Cement	0/4 Sand	Water	w/c ratio
Mortar	566	1344	270	0.43
Cement paste	1338	0	575	0.43

One mortar and one cement paste prisms with dimensions 4 × 4 × 16 cm^3 were cast in polypropylene molds to avoid any presence of metallic compounds from the molds. After one

117 day of curing under sealed conditions in an air-conditioned room at a temperature of 20°C and
118 90% RH, the specimens were unmolded and further cured in lime-saturated water until the age
119 of 28 days.
120 After 28 days, a 1.5 cm-thick 4 × 4 cm^2 slice was cut in the center of the specimen using a
121 precision saw. The samples were cut again to obtain a 1.5 × 2.0 × 2.0 cm^3 cubic specimen.
122 These two specimens were embedded in resin and automatically polished before the indentation
123 measurements. Mortar specimen and cement paste samples were polished with Si-C paper with
124 decreasing particle size (500, 1200, 2000, 4000 grit) using alcohol-based polishing liquid to
125 avoid any reaction with unhydrated cement particles. Polishing times were selected from some
126 seconds (500 paper) to around some minutes per paper (4000 paper) to limit the risk of
127 aggregate cracking. Finally, the samples were polished using 1 µm diamond paste for 15
128 minutes. A root mean square of the surface roughness (Rq) of around 200 nm, resp. 80 nm, was
129 measured for the mortar, resp. cement paste sample.
130
131 2.1.2 Grid indentation tests

132 To investigate representative surfaces of the mortar sample and the cement paste sample resp.,
133 microindentation and nanoindentation tests were performed using a Berkovitch indenter
134 (Bruker TS 77) probe over a grid of 40 x 40 points (1600 indents), evenly spaced by 500 µm,
135 2 µm resp. For each indent, the load was increased linearly over time in 5 s up to 500 mN, resp.
136 1 mN, kept constant during the 100 s holding phase, and decreased linearly over time in 5 s.
137 The short loading time was selected to limit creep during this period and did not damage the
138 sample (as checked under a microscope of an SEM after indentation). In total, the test lasted
139 around four days to perform the entire grid, which motivates the development of a faster yet
140 reliable method to assess the mechanical behavior of heterogeneous materials. Typical

141 indentation curves of the two major phases in the mortar sample and the cement paste samples
142 are represented in Fig. 1.
143

a)

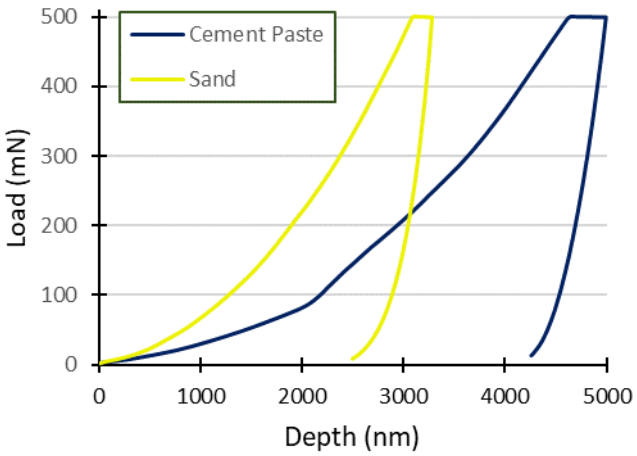

b)

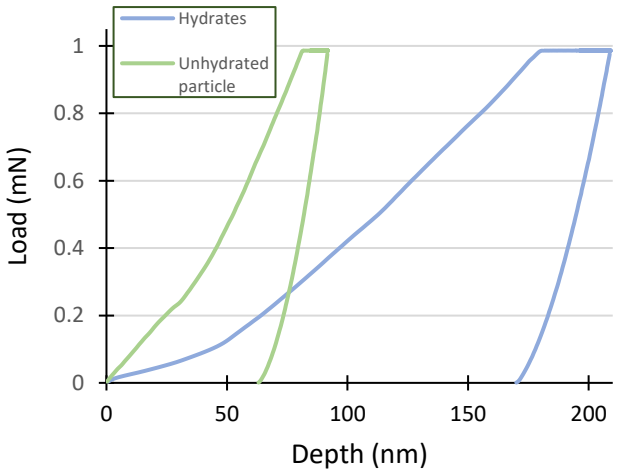

144 **Fig. 1.** Typical indentation curves: a) cement paste and sand phases in the mortar specimen, b)
145 hydrate and unhydrated particle in the cement paste..
146

147 Reduced modulus E_r and indentation hardness H_{IT} were calculated according to equations (1)
148 and (2):

$$E_r = \frac{1}{2}\sqrt{\frac{\pi}{A_c}}S \quad (1)$$

149

$$H_{IT} = \frac{P_{max}}{A_c} \quad (2)$$

150 Where A_c is the projected contact area and S the slope of the unloading curve using Oliver and
151 Pharr approach [7]. No specific filtering was performed on the indentation curves to represent
152 a general indentation acquisition.

153

154 2.1.3 Acquisition of indented area image and generation of representative artificial images

155 Photographs of the indented zone were acquired after indentation to visually identify indent
156 location or, resp., deduce indent location, in the case of the mortar and cement paste specimens
157 resp.

158 As illustrated in Fig. 2 (a), a picture of the indented zone on the mortar sample has been obtained
159 using a Hirox RH-2000 3D microscope by merging around 200 3D reconstructed images evenly
160 spaced along the indented area using a 140× magnification leading to a final horizontal
161 resolution of the 2D projected image of 1.5 µm / pix that is adequate to locate the indents and
162 assess their nature. The high proportion of sand particles of various sizes, creating an optimized
163 granular skeleton typical of high-performance concrete, is worth noting.

164 As illustrated in Fig. 2 (b), a SEM image of the cement paste sample was obtained using an
165 acceleration voltage of 15 kV and a working distance of 7 mm and a low vacuum pressure of
166 60 Pa to limit the risk of cracking. A relatively large light gray unhydrated particles was found
167 in the left part of the indented zone, while four smaller unhydrated particles were located in the
168 right part of the image. Most of the indents were not visible due to the relatively small load

169 compared to the roughness of the sample, except some small imprints on the unhydrated
170 particles.
171
172

a)

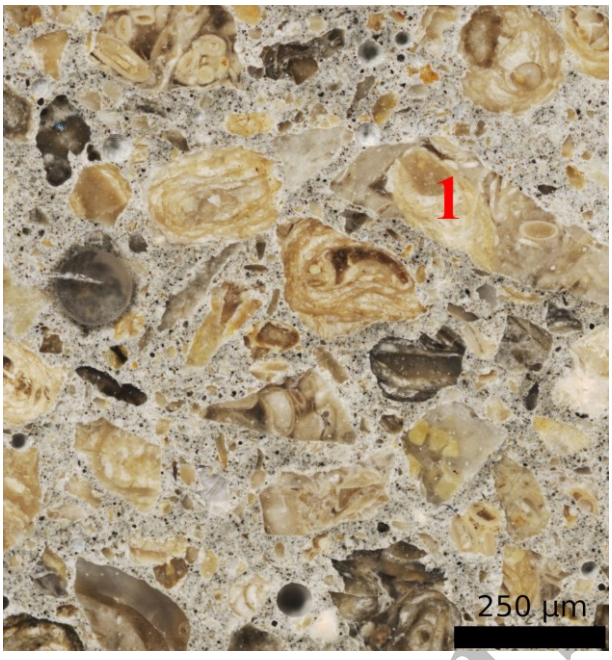

b)

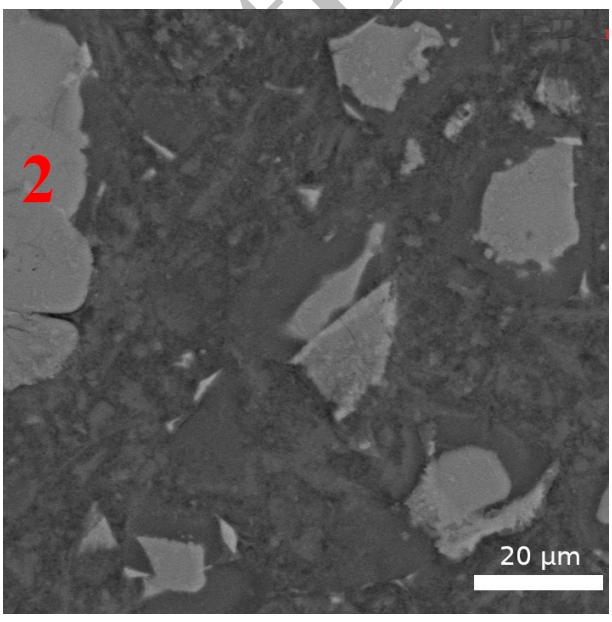

Fig. 2. Microscopic image of the samples: a) 2D optical microscopic image of mortar sample with one sand particle labeled 1 (1cm × 1cm zone indented using a 40 × 40 matrix of 500mN indents), b) SEM image of cement paste sample with one unhydrated particle labeled 2 (80µm × 80µm zone indented using a 40 × 40 matrix of 1 mN indents (indents are not visible)).

2.2 Numerical methods

2.2.1 Kriging

Initial values, either indent nature based on the microscopic images or indentation curves, were acquired initially before running the ε-greedy procedure in order to gain initial knowledge before inferring the unknown indent nature using Gaussian Process Classification. To this end, an initial regular Kriging stage has been performed with various Kriging parameters from K=2 (half of the indents were initially artificially performed) to K=20 (1/20th of the indents were selected). The initial sampling sets for the different Kriging parameters are illustrated in Fig. 3. Considering the maximum possible number of indents being 1600 (40 x 40), the initial number of indents after the initial Kriging stage ranged from 80 (K=20) to 800 (K=2).

a) K=2

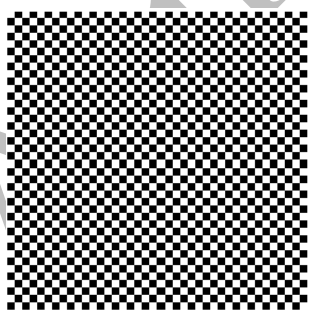

b) K=3

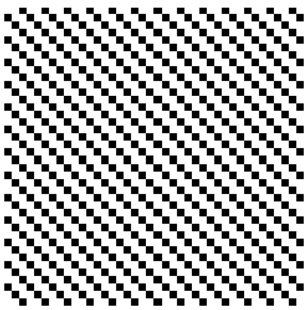

c) K=4

d) K=6

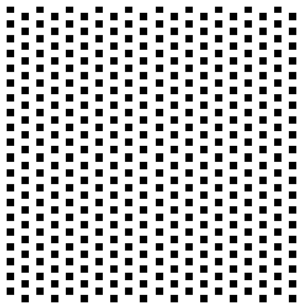

e) K=8

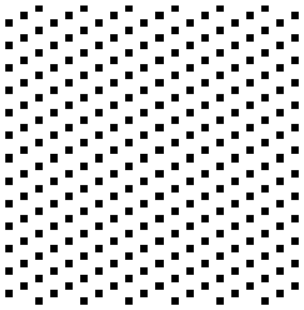

f) K=12

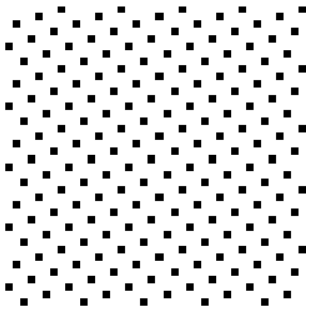

g) K=16

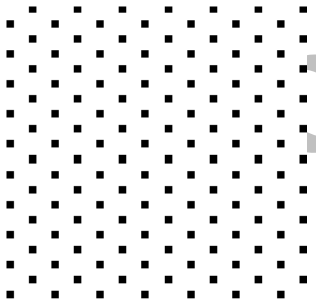

h) K=20

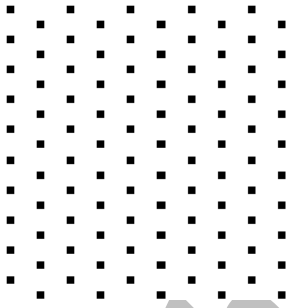

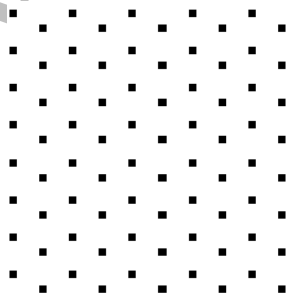

188 **Fig. 3.** Initial sampling sets of indents performed on the sample using various Kriging
189 parameters (dense to loose Kriging): a) K=2, b) K=3, c) K=4, d) K=6, e) K=8, f) K=12, g)
190 K=16, h) K=20.

191

192 2.2.2 Gaussian Process Classifier

193 After the initial Kriging stage, and regularly during the algorithm iterations, Gaussian Process
194 (GP) classifiers were used to infer the nature of unknown indents based on the knowledge of
195 the nature of the surrounding indents. GP classifiers [42] are non-parametric classifiers, relevant
196 to the resent problem as they require few examples to perform correctly. Given data points x_i

from a domain X with corresponding class labels y_i in $[-1; +1]$, one would like to predict the class membership probability for a test point x. This is achieved using a latent function f whose value is mapped into the unit interval employing a sigmoid function $\sigma : \mathbb{R} \longrightarrow [0; 1]$, used because of its desirable mathematical properties, such that the class membership probability $P(y = +1 \,|x)$ can be written as $\sigma(f(x))$. Under some conditions , the likelihood can be written as $P(y \,|x) = \sigma(yf(x))$.

A GP [42] is a stochastic process fully specified by a mean function $m(x) = E[f(x)]$ and a positive definite covariance function $k(x, x') = V[f(x), f(x')]$. This means that a random variable $f(x)$ is associated with every x in X , such that for any set of inputs X, the joint distribution $P(f \,|x) = \mathcal{N}(f|m_0, K)$ is Gaussian with mean vector m_0 and covariance matrix K, conveniently termed kernel.

The factorial likelihood being non Gaussian, the posterior over the latent values is also not Gaussian. In this paper, the Laplace approximation is used for approximating the non-Gaussian posterior by a Gaussian.

Assuming without loss of generality $m_0 = 0$, one still has to define K, whose design will enforce specific properties of the metric space of X. Kernels encode the assumptions on the function being learned by defining the 'similarity' of two x_i combined with the assumption that similar x_i should have similar target values.

Among the wide range of kernels available, the most common stationary and non-stationary kernels with a small number of parameters have been tested in this paper: the Radial Basis Function (RBF) kernel with its rational quadratic extension, the Matern one and the Dot Product kernel. The combination of Matern and Dot Product kernels, and Matern and Dot Product squared have been also evaluated.

The RBF kernel is the most commonly used kernel and also known as the 'squared exponential' kernel and is given by the following:

$$k(x_i, x_j) = \exp\left(-\frac{d(x_i, x_j)^2}{2l^2}\right) \quad (3)$$

Where $d(\cdot,\cdot)$ is the Euclidean distance and l a length-scale parameter.

The matern kernel is a generalization of the RBF. It has an additional parameter that controls the smoothness of the resulting function. When set to 3/2 it ensures that the functional function is differentiable at least once, and gives:

$$k(x_i, x_j) = \left(1 + \frac{\sqrt{3}}{l} d(x_i, x_j)\right) \exp\left(-\frac{\sqrt{3}}{l} d(x_i, x_j)\right) \quad (4)$$

The RationalQuadratic kernel is given by the following:

$$k(x_i, x_j) = \left(1 + \frac{d(x_i, x_j)^2}{2\alpha l^2}\right)^{-\alpha} \quad (5)$$

Where α is a scale mixture parameter.

This kernel can be seen as a scale mixture of RBF kernels with different characteristic length-scales. It is parameterized by a length-scale parameter l and a scale mixture parameter α that must both be positive.Those kernels are termed stationary because they depend solely on the radial distance between x_i.

The last kernel evaluated in this study was the dot product kernel. Conversely, the dot product is a non-stationary kernel as it depends on the value of the input coordinates themselves:

$$k(x_i, x_j) = \sigma_0^2 + x_i \cdot x_j \quad (6)$$

This kernel is parameterized by the σ_0 parameter. The dot product kernel is commonly conbined with exponentiation. For this reason, Matern + Dot Product and Matern + Dot Product^2 have been studied herein. For all tested configurations, kernel parameters were optimized during the training procedure.

2.2.3 ε–greedy algorithm for indents location selection

2.2.3.1 Prediction using indents nature identified by microscopic images as priors

The methodology diagram reported in Fig. 4 describes the algorithm that considers the indents nature identified by microscopic images (offline algorithm) as priors to predict the next indent to be performed. After an initial Kriging step, the nature of the selected indents, either the phase of interest or not, was obtained based on microscopic image analysis through greyscale thresholding in the case of the cement paste or manual annotation in the case of the mortar specimen (due to the low contrast between cement paste and sand particles). Using this information, a GP classifier was then used to infer the nature of the other indents in the indentation map. Based on this inference, the next indents to perform were selected following an ε–greedy strategy, i.e., 80% of the indents was selected greedily where the GPC predicted the highest probability of finding the phase of interest and 20% of indents was selected according to an exploration strategy whose influence will be discussed in the results. The nature of these indents has been assessed using microscopic images and the sequence 'indents nature verification – GPC – ε-greedy strategy' process has been repeated during tens of steps to perform as many indents as possible in the phase of interest given the indentation zone. The main goal of this algorithm was to independently study as many parameters as possible from GPC and the ε-greedy strategy. The influence of these parameters will be discussed in section 3.1.

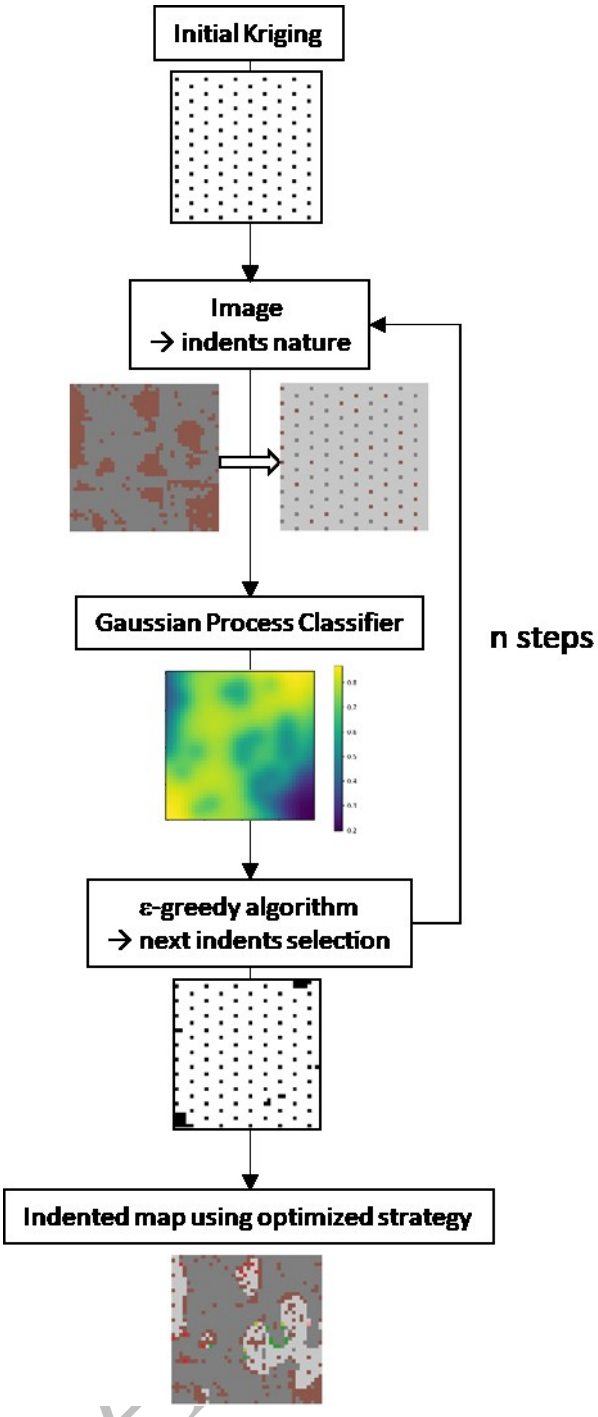

260

261 **Fig. 4.** Flowchart of the ε–greedy algorithm for indents location selection using geometrical

262 information.

263 *2.2.3.2 Algorithm using indentation curves without geometrical information*

264 The methodology diagram reported in Fig. 5 shows the principle of the full-fledged algorithm

265 that performs online estimation of phase of interest. This algorithm could be implemented on

indenters to locate as many indents as possible in a phase of interest during the indentation of a heterogeneous material. After an initial rather loose Kriging step, the nature of the selected indents was inferred using unsupervised clustering (k-means) performed on the calculated micro-mechanical properties The unsupervised algorithm inputs were E_r and h_{max}, the maximum penetration depth for the mortar specimen and E_r and H_{IT} in the case of the mortar, resp. cement paste specimen to guarantee the convergence of the overall procedure in both cases. k-means algorithm has been randomly initialized ten times, and convergence has been obtained during the first 300 runs with a relative tolerance of 1e-4 with regards to Frobenius norm. Three classes were estimated corresponding to indents in a) the phase of interest, b) indents in the other phase and c) indents with intermediate properties, likely located at interfaces. The latter two classes were grouped considering indents should not be similar to these indents. Based on this information, a GP classifier was then used to infer the nature of all the indents in the indentation map. From this inference, the next indents to perform were selected following the same ε–greedy strategy as described in the previous section, i.e., 80% of the indents were selected greedily where the GPC predicted the highest probability of finding the phase of interest and 20% of indents were selected according to an exploration strategy. The nature of these indents has then been assessed using unsupervised clustering, and the overall 'indents nature verification – GPC – ε-greedy strategy' process has been repeated during tens of steps to perform as many indents as possible in the phase of interest in the indentation zone.

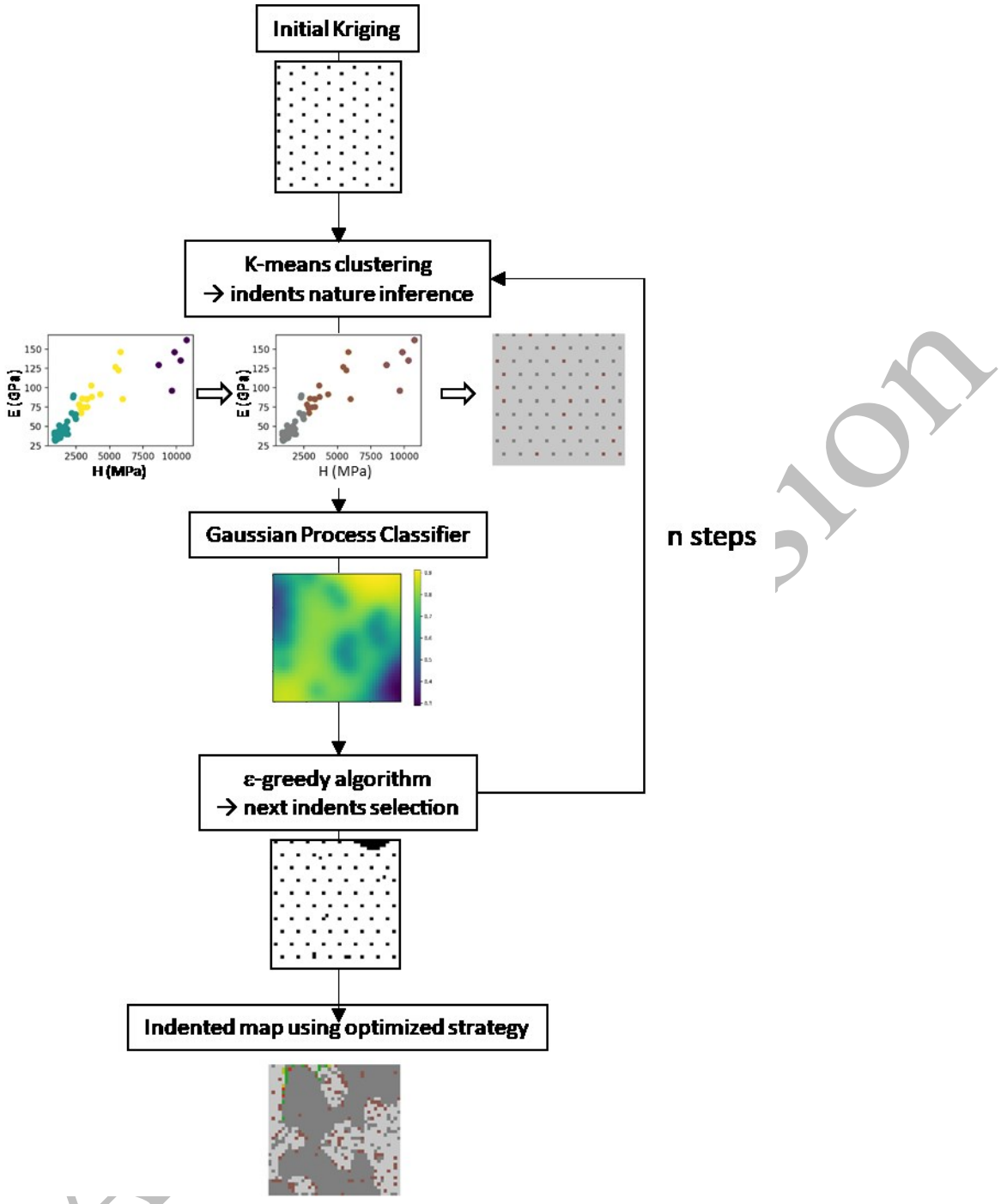

285

286 **Fig. 5.** Flowchart of the ε–greedy algorithm for indents location selection using indentation

287 curves.

288

3. Results and discussion

3.1 Algorithm using geometrical information only

3.1.1 Convergence of the algorithm

The efficiency of the ε-greedy algorithm using indent nature given by a microscopic image has been validated for the microindentation test of the mortar sample and the nanoindentation test of the cement paste sample. As illustrated in Fig. 6, after the first initial Kriging stage that provides information about the nature of about 100 indents located on the area of interest, the proposed algorithm was able to detect zones with higher probabilities of finding indents of interest. The exploration-exploitation strategy automatically then selected the next indents to perform. The algorithm has been run during several steps, typically from 20 to 50 steps, selecting 20 indents (1.25% of the total number of indents) greedily at each step. Those indents are selected as the ones with the highest probability of locating paste or hydrates areas in the case of the mortar sample, cement paste sample, resp. Additionally, 5 indents have been selected according to the exploration strategy.

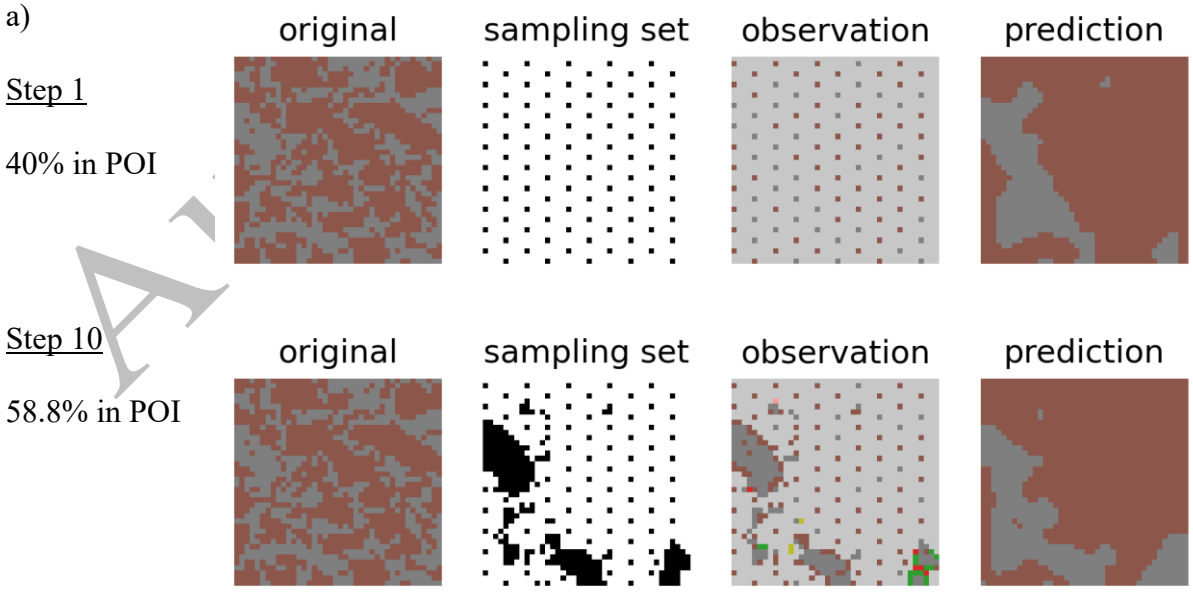

Step 20

56.1% in POI

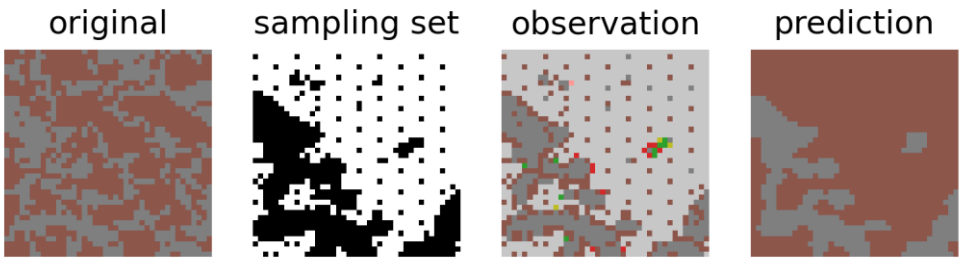

Step 30

56.2% in POI

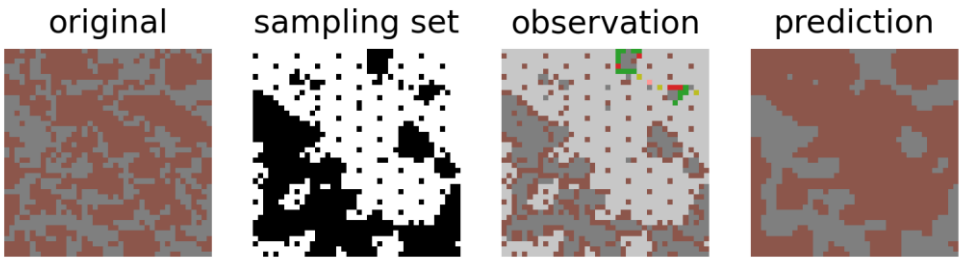

Step 40

56.0% in POI

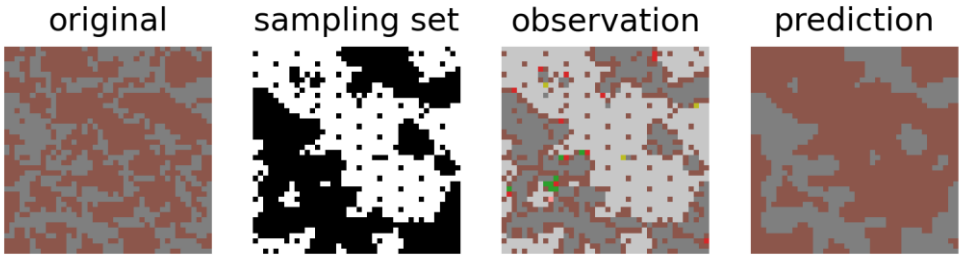

Step 50

55.6% in POI

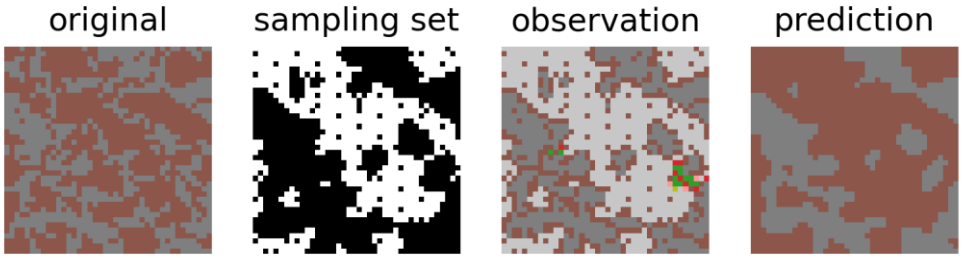

b)

Step 1

69.0% in POI

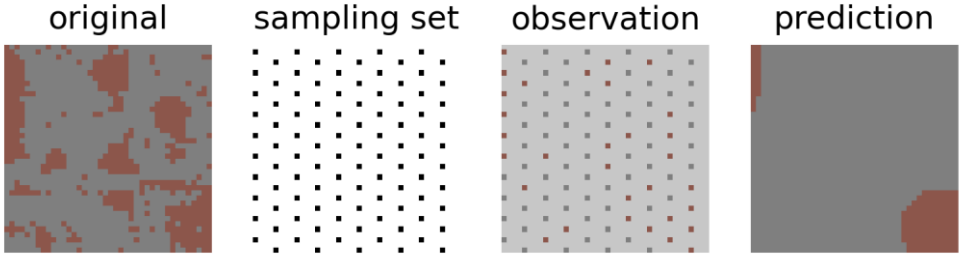

Step 10

84.9% in POI

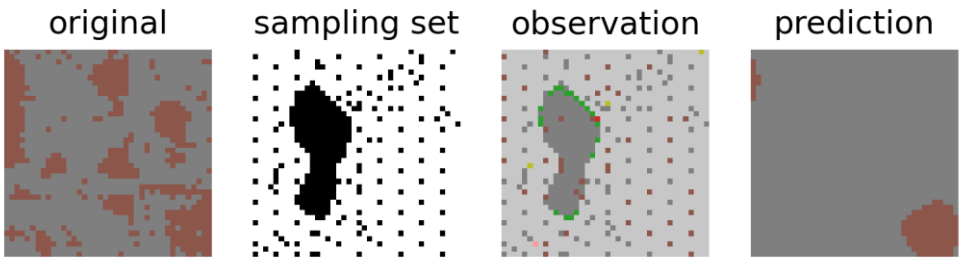

Step 20

87.8% in POI

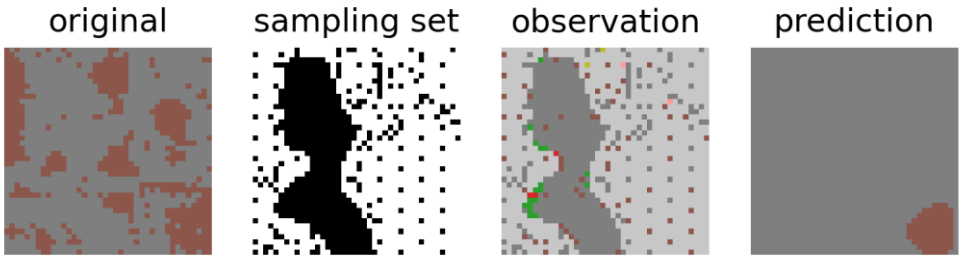

Step 30

86.5% in POI

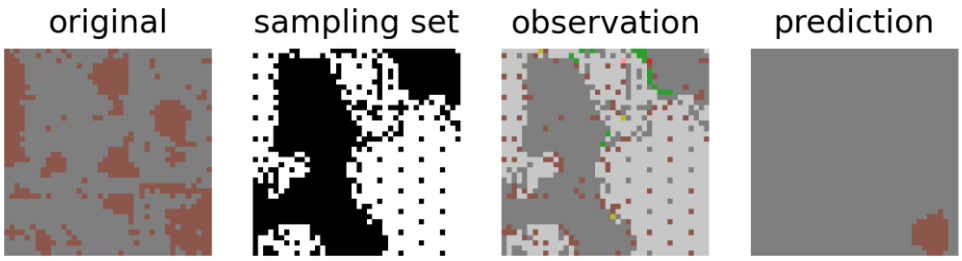

Step 40

86.5% in POI

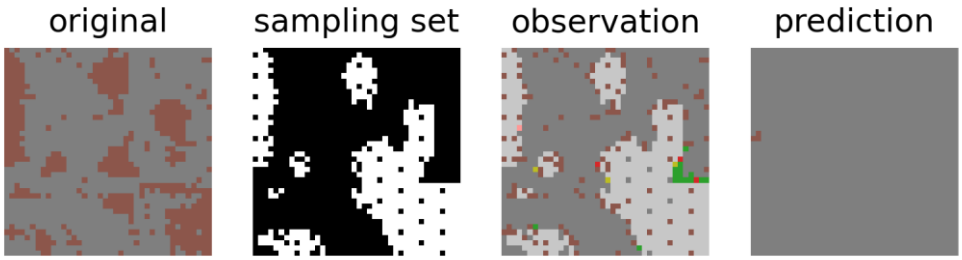

Step 50

84.6% in POI

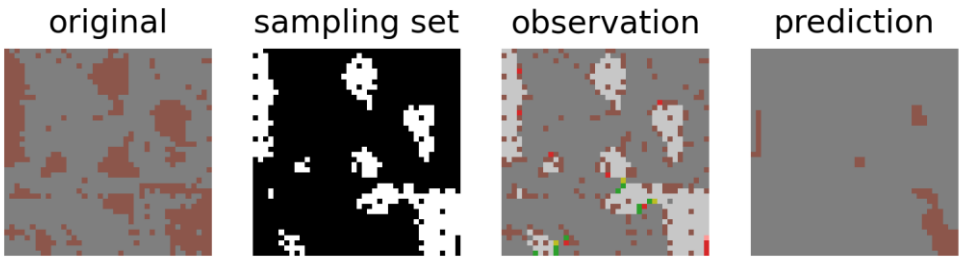

Legend:

indent in the phase of interest

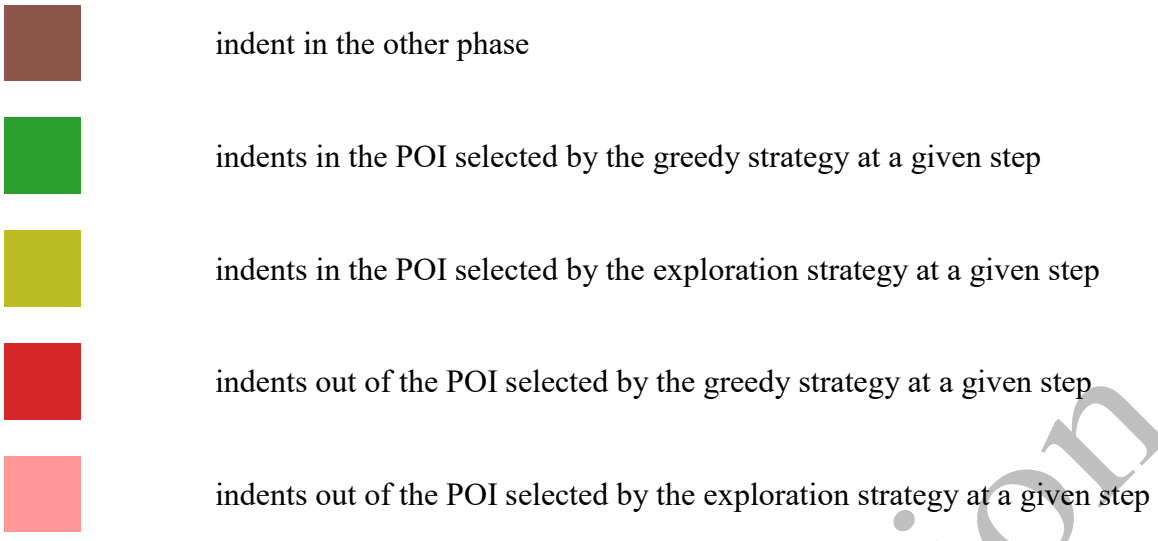

Fig. 6. Maps of the selected indents over time with Kriging parameter equal to 16, GPC kernel Matern + DotProduct: a) mortar sample, b) cement paste sample. Proportion of indents in the phase of interest (POI) is reported at each step.

More specifically, in the case of the mortar sample illustrated in Fig. 6 (a), an initial Kriging stage with a sampling parameter equal to 16 leads to. 100 indents to be performed on the surface out of the 1600 possible indents. Then, the GP classifier predicted paste indents in the left part of the area, notwithstanding the relative lack of precision in the prediction (even if GPC training accuracy was around 0.850 to 0.910). The relative lack of precision of the initial prediction, which was a result of a tradeoff chosen to increase execution speed, was not found to limit the overall capability of the model to find zones in the phase of interest. The algorithm then greedily located the next indents in this zone. Most of these first indents corresponded to paste indents according to the microscopic images, GPC predictions were then refined using these indents nature and more indents were performed in the uncovered area during the first iterations of the algorithm. Due to the appropriate exploration strategy, whose influence will be discussed in the next section, some indents were performed in the bottom part of the area between steps 5 and 10, and in the top part of the area between 10 and 15. Because some of these exploratory indents corresponded to paste zones, GPC predictions were revised with new information and high

probabilities of finding paste indents were found in some of these specific zones, leading to the testing of close areas according to the greedy strategy. Therefore, new areas containing paste were found using the exploratory strategy. Several paste zones could be found on the sample even though the maximum 'resolution' of the indented map was relatively poor and the overall area contained a small proportion of the phase of interest, e.g., cement paste, as opposed to the other phase sand aggregates (around 40% and 60% resp.).

In the case of the cement paste sample, the overall area contained a higher proportion of hydrates, the phase of interest, as opposed to the other phase, the clinker particles, corresponding to regularly spaced particles (69% and 31% resp.). For this reason, the algorithm effectively found where to locate indents corresponding to the phase of interest and a relatively good initial prediction of the position of clinker particles was made by GPC after the initial Kriging stage, as illustrated in Fig. 6 (b). The locations selected by the greedy strategy to perform indents corresponded to hydrate areas located far away from the clinker phases leading to a good efficiency during the first steps. Due to the exploration strategy, several initial positions were found to generate kernels of indents in the phase of interest as in the previous case. Therefore, between strep 5 and 30, three clusters containing a high proportion of the phase of interest were found, one in the top right part of the area, one in the middle left part, and one in the bottom part. Then, it was observed that the greedy exploitation strategy recommended performing indentations at the borders of these clusters leading to their extension as long as indents were performed in the phase of interest. Finally, the algorithm found most of the phase of interest and indents location was selected by the algorithm around the clinker particles, as it can be seen at steps 40 and 50.

The algorithm's efficiency has been evaluated by measuring the proportion of indents in the phase of interest relative to the ratio of indents tested in the area. As illustrated in Fig. 7, in both the mortar and cement paste cases, the proportion of indents located in the phase of interest

quickly increased from the value obtained after the initial random Kriging (40% and 69% for mortar and cement paste sample, resp.) to around 58% and 88% for the mortar and cement paste samples, resp. At each step, the proportion of indents in the phase of interest, 58% and 87% on average for the mortar and cement paste resp. (for proportions of tested indents smaller than 40% and 70% resp.), was higher than the random proportion of the phase of interest in the entire area, 42% and 71% for the mortar and the cement paste, resp., as illustrated in the right-side figures. After around 60% of the indents location in the cement paste (Fig. 7 b) were tested, a drop in the overall efficiency associated with highly variable instantaneous precision can be observed in the case of the cement paste (Fig. 7 b). This drop can be explained because most indents in the face of interest have been found (and the global objective fulfilled).

a)

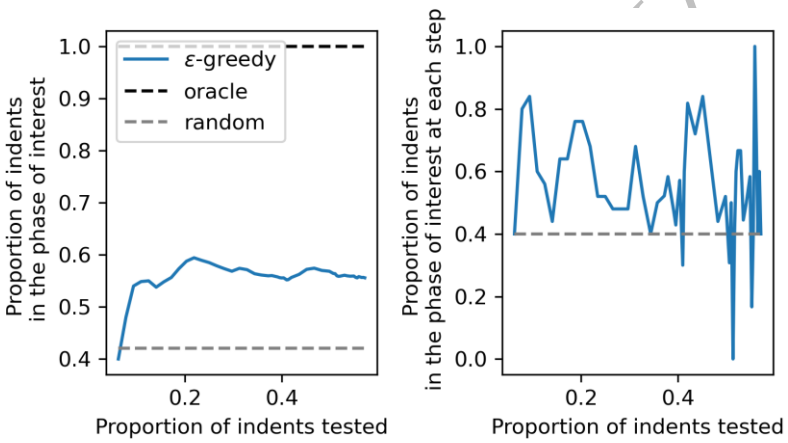

b)

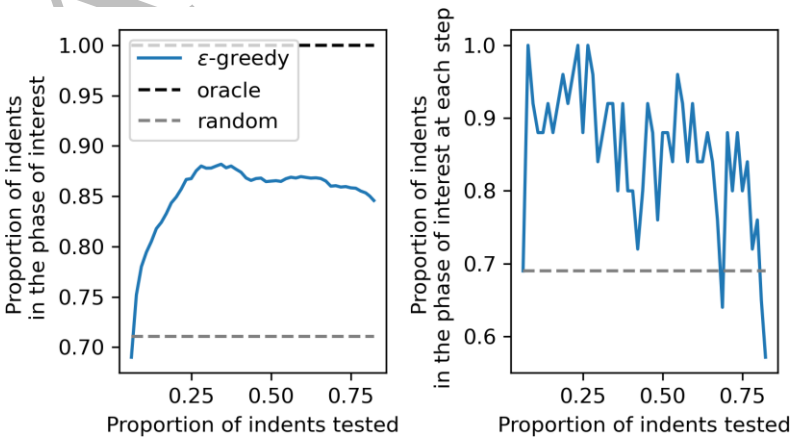

Fig. 7. Typical evolution of indents in the phase of interest over time: a) mortar, b) cement paste

3.1.2 Influence of initial Kriging parameters.

The influence of the initial Kriging parameters has been assessed by running the algorithm using several Kriging parameters (K) from K=2 to K=20 in the two cases. As illustrated in Fig. 8, in both cases, the maximum proportion of indents in the phase of interest globally increased with increasing K values. This observation can be explained because random initial Kriging relative importance decrease with increasing K values. For example, in the case K=2, half of the possible indents (800/1600) were performed randomly during the initial Kriging phase, explaining the relatively small room for improvement when the ε-greedy algorithm is then activated. However, it is worth noting that the exploration-exploitation algorithm could select indents in the phase of interest in both the mortar and the cement paste cases after an initial Kriging stage with K=2, because of the information gathered during the Kriging stage.

a)

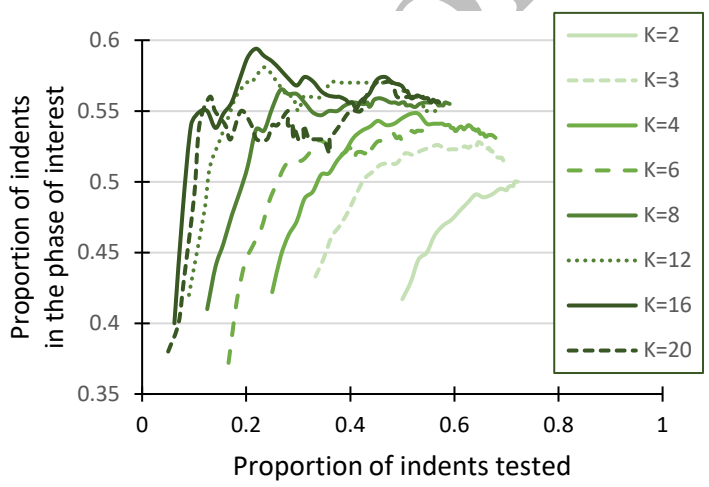

b)

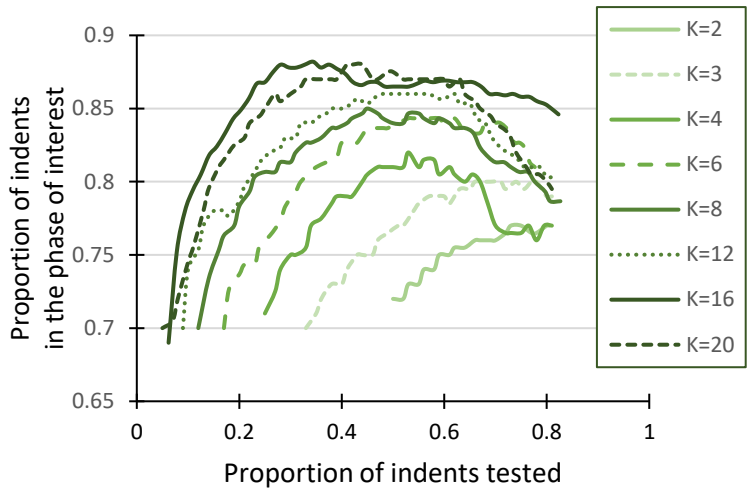

Fig. 8. Evolution of indents in the phase of interest over time for several initial Kriging parameters : a) mortar specimen, b) cement paste specimen.

The maximum proportion of indents in the phase of interest increased from K=2 to K=12 and from K=2 to K=16 in the case of the mortar specimen, resp., cement paste specimen, while the performance curves were similar for higher values of K. This highlights the increasing algorithm's efficiency, and optimal K values of around 16 can be selected. With K=16, only 6.25% of the indents were performed during the initial random Kriging stage. Then, the exploration-exploitation algorithm determines where to perform the next indents, and the proportion of the indents in the phase of interest quickly grew and remained relatively stable even though only 20 to 40% of the indents were performed (320 to 640 indents over 1600 possible indents, corresponding to a standard number of indents in statistical nanoindentation of heterogeneous materials). In the case of the mortar (Fig. 8 a), the performance of the algorithm with an initially loose Kriging (K=20) is decreased compared to K=16. There is not enough information to infer the indents' nature to start the exploration of the regions with the highest proportions of the phase of interest, and auxiliary inputs such as the phase proportion could help the algorithm initiation.

3.1.3 Exploration strategy adaptation

The exploration strategy is an essential factor affecting ε-greedy algorithms' performance. For this reason, three strategies have been evaluated with the ratio between exploration and exploitation being constant equal to 20% (5 and 20 indents resp.):

i) strategy 1: most uncertain not-of-interest phase positions (sand or clinker particles) were selected to perform indents to obtain information at the boundary between the phase of interest and the other phase,

ii) strategy 2: most uncertain phase of interest positions were selected to obtain a similar kind of information but with a higher probability of selecting positions of the phase of interest and,

iii) strategy 3: particular phase of interest positions, i.e., positions where the probability of finding the phase of interest was higher than 75% or higher than 55% if no position associated with probability >75% was found, were tested randomly (conservative exploration strategy).

Strategy n°3 was considered an intermediate option between strategies 1 and 2, specifying probabilities of finding the phase of interest though keeping some randomness aspect. Recent works suggest promising exploration strategies optimization during the learning process, which would be relevant to implement in future studies [43,44]. As illustrated in Fig. 9 (a), the exploration strategy did not influence the algorithm's performance in the case of the mortar sample. This could be due to the relatively small number of positions with probabilities of finding the phase of interest higher than 75%. Therefore, the three exploration strategies selected similar indents. Conversely, in the case of the cement paste sample, exploration strategy 3 performed better than the other strategies as illustrated in Fig. 9 (b). This can be attributed to the effective selection of the locations to explore. They mostly corresponded to the phase of interest located relatively to positions tested by the greedy algorithm. Then, new

412 ‘seeds’ can be selected on the indentation map to find new positions where the phase of interest
413 was located, as illustrated in Fig. 6 (b).

a)

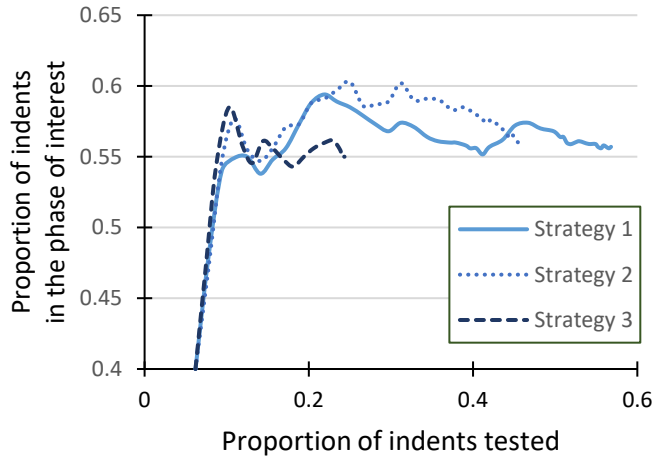

b)

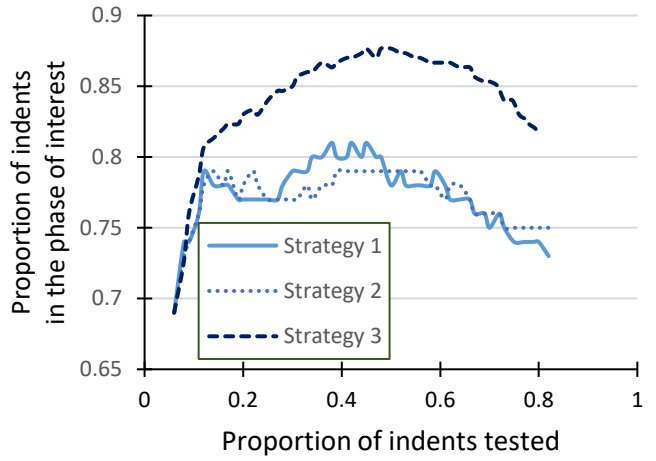

414 **Fig. 9.** Evolution of indents in the phase of interest over time for several initial Kriging
415 parameters : a) mortar sample, b) cement paste sample.

416

417 3.1.4 Kernel selection

418 The influence of the kernel used with the GP Classifier has been assessed. As illustrated in Fig.
419 10, most of the tested kernels performed well except the DotProduct kernel that did not lead to

satisfactorily convergence in the cement paste case and led to a smaller maximum proportion of indents in the phase of interest and a slower increase of this proportion in the mortar case. Some kernels did show promising results in both cases, e.g., Matern + DotProduct and, with slightly more variable results, Matern + DotProduct^2 and RationalQuadratic. For this reason, most of the simulations reported in this manuscript were performed using Matern + DotProduct or Matern + DotProduct^2 kernels.

a)

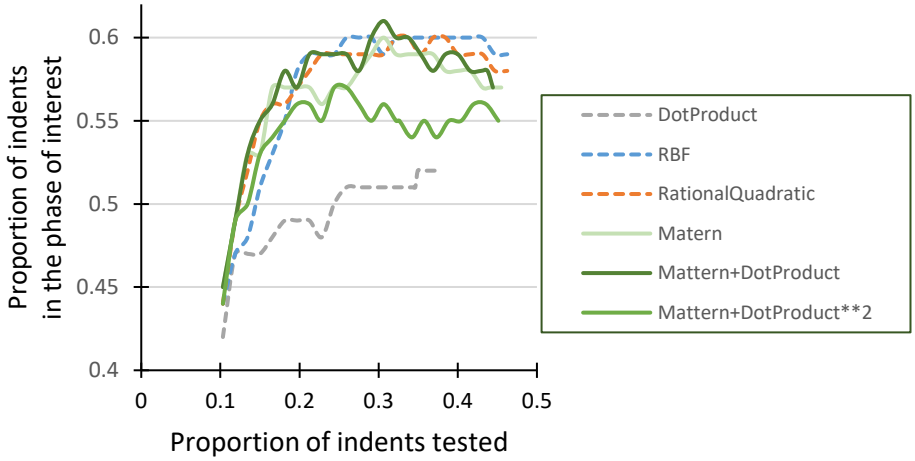

b)

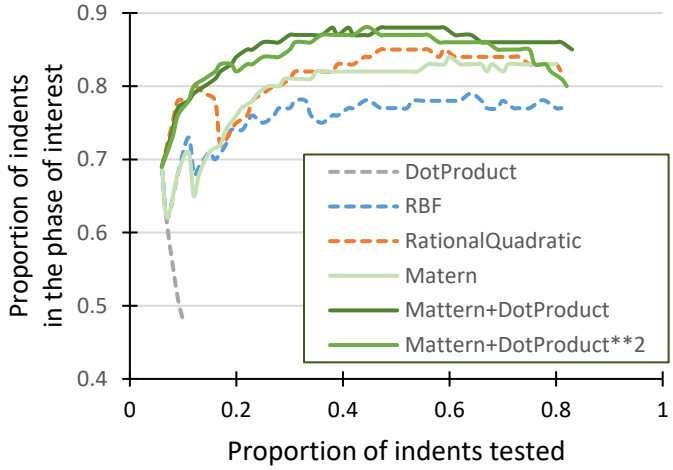

Fig. 10. Evolution of indents in the phase of interest over time for several kernel natures and parameters: a) mortar sample, b) cement paste sample.

3.2 ε–greedy algorithm using priors from indentation curves only

3.2.1 Deconvolution of indentation curves

The effectiveness of deconvolution after the initial Kriging step has been evaluated to build an algorithm that considered indentation curves to get rid of the need of geometrical information as defined in section 2.2.3.2 to predict the prior information regarding the phase of the existing indents. As illustrated in Fig. 11, the indentation curves can be correctly clustered into three groups by an unsupervised algorithm in the case where K=16 whatever the micro-mechanical properties used as inputs (E_r and h_{max}, the maximum penetration depth for the mortar specimen and E_r and H_{IT} in the case of the mortar, resp. cement paste specimen). The clusters obtained using 100 curves ($1/16^{th}$ of the 1600 curves) illustrated in Fig. 11 (b) and (d) were very similar to the clusters obtained using half of the curves in both the mortar and the cement paste cases (K=2). The reduced modulus cluster center value of the phase of interest was 30.4 GPa and 30.0 GPa in the case of the mortar specimen with K=16 and K=2 resp., which corresponds to broadly reported values of cement paste properties [16] and 43.3 GPa and 43 GPa in the case of the hydrates properties in the cement paste for K=16 and K=2 resp. Although slightly elevated, these last two values were very close to each other and are in the order of magnitude of the reported values for the cement paste hydrates (high-density CSH with indentation modulus values close to 30 GPa and portlandite with values close to 42 - 44 GPa [45]).
Therefore, clustering of initial curves obtained through Kriging can provide sufficient information, and the same algorithm trained once can be used for the entire ε-greedy procedure.
In case of a very loose initial Kriging or an important number of phases, the clustering algorithm

could be trained several times during the algorithm or consider information from similar materials.

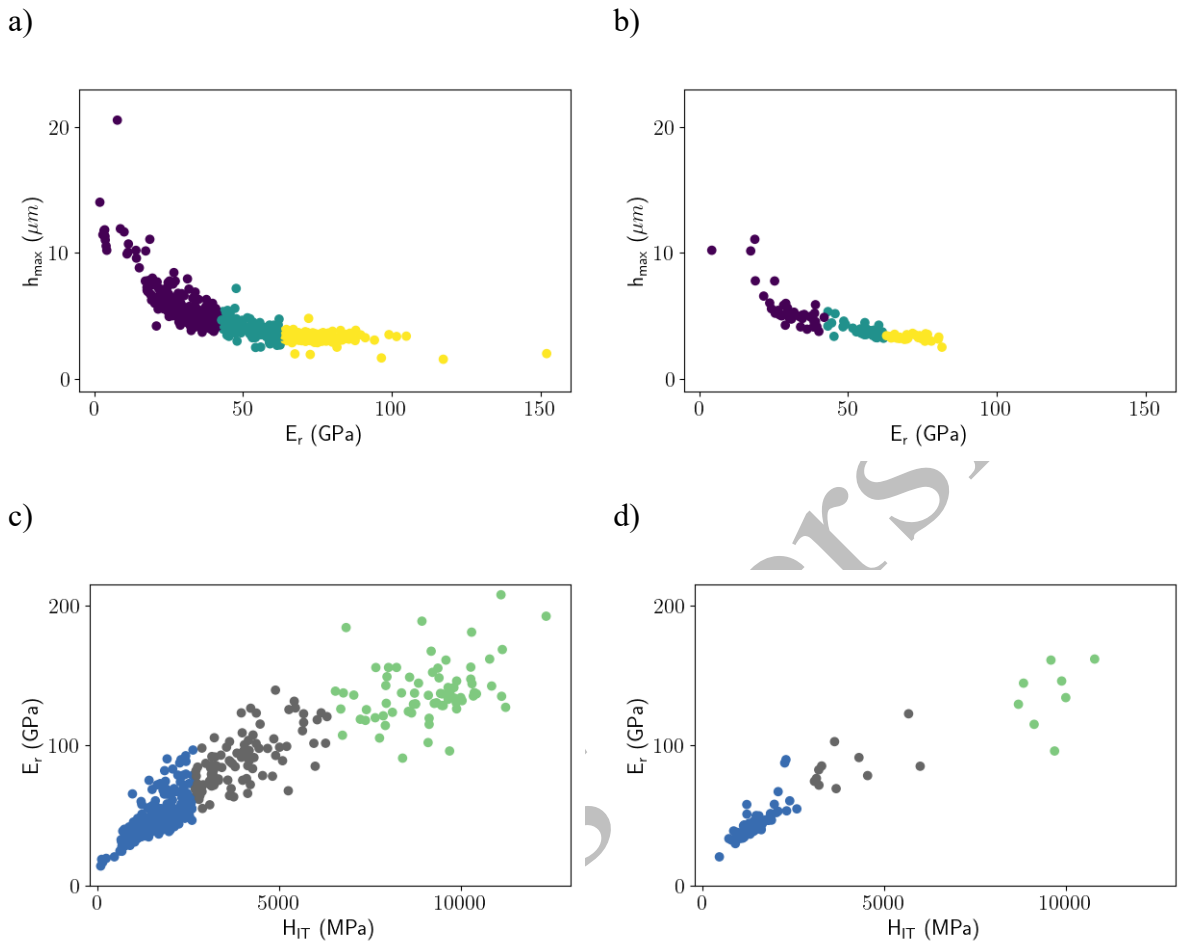

Fig. 11. Deconvolution results of the indentation curves after the initial Kriging step: a) mortar sample with K=2, b) mortar sample with K=16, c) cement paste sample with K=2, d mortar sample with K=16

3.2.2 Convergence of the algorithm

The online algorithm, using indentation curves only, showed excellent convergence results with the aforementioned optimized parameters. After unsupervised clustering using the indentation curves as detailed in the previous paragraph, the GP classifier has been used to infer the indents' nature based on the clustering results and the ε-greedy procedure has been applied to select the

461 next indents. As illustrated in Fig. 12, the algorithm was able to find the zones with the highest

462 probabilities of finding indents in the phase of interest during 30 to 50 steps.

a)

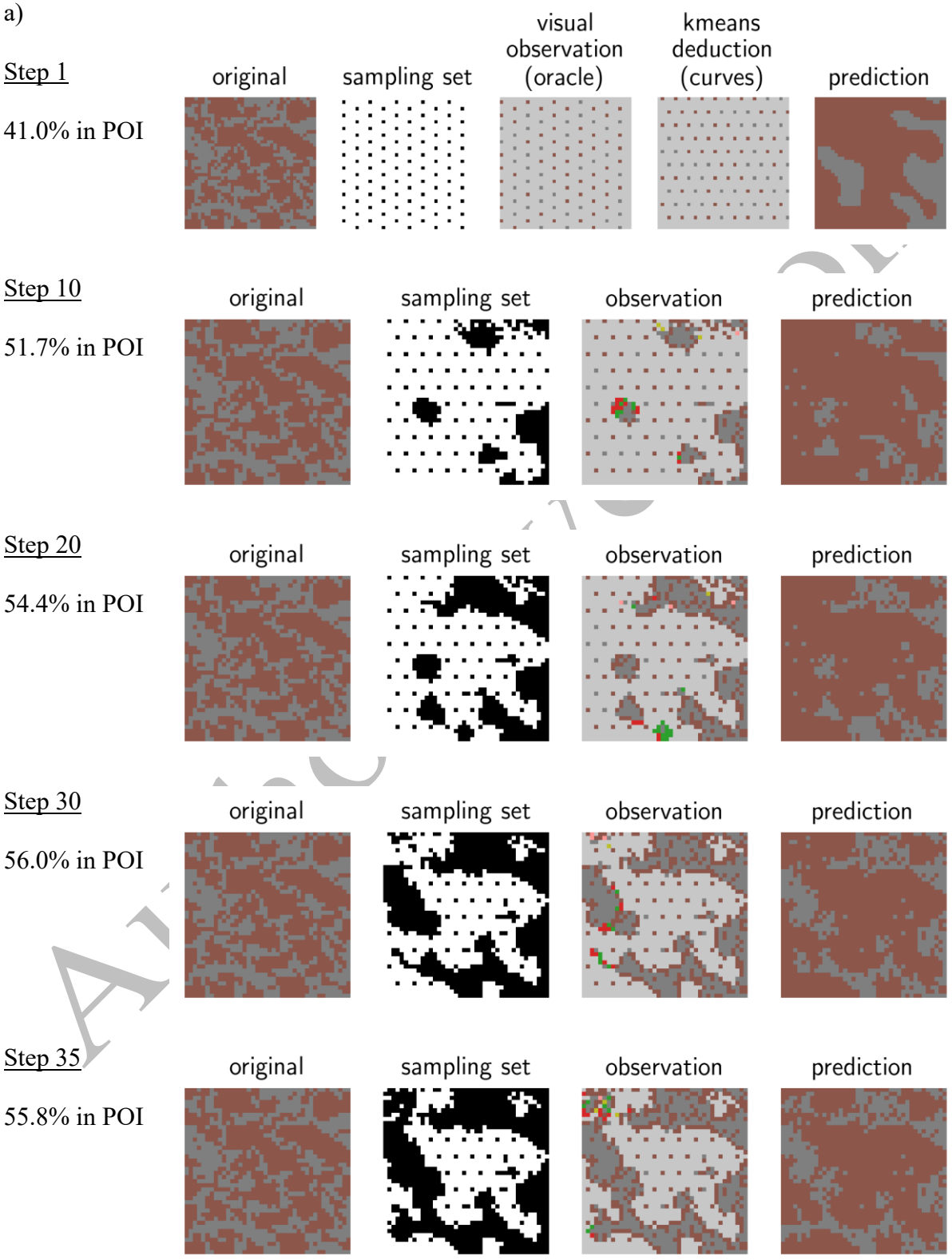

b)

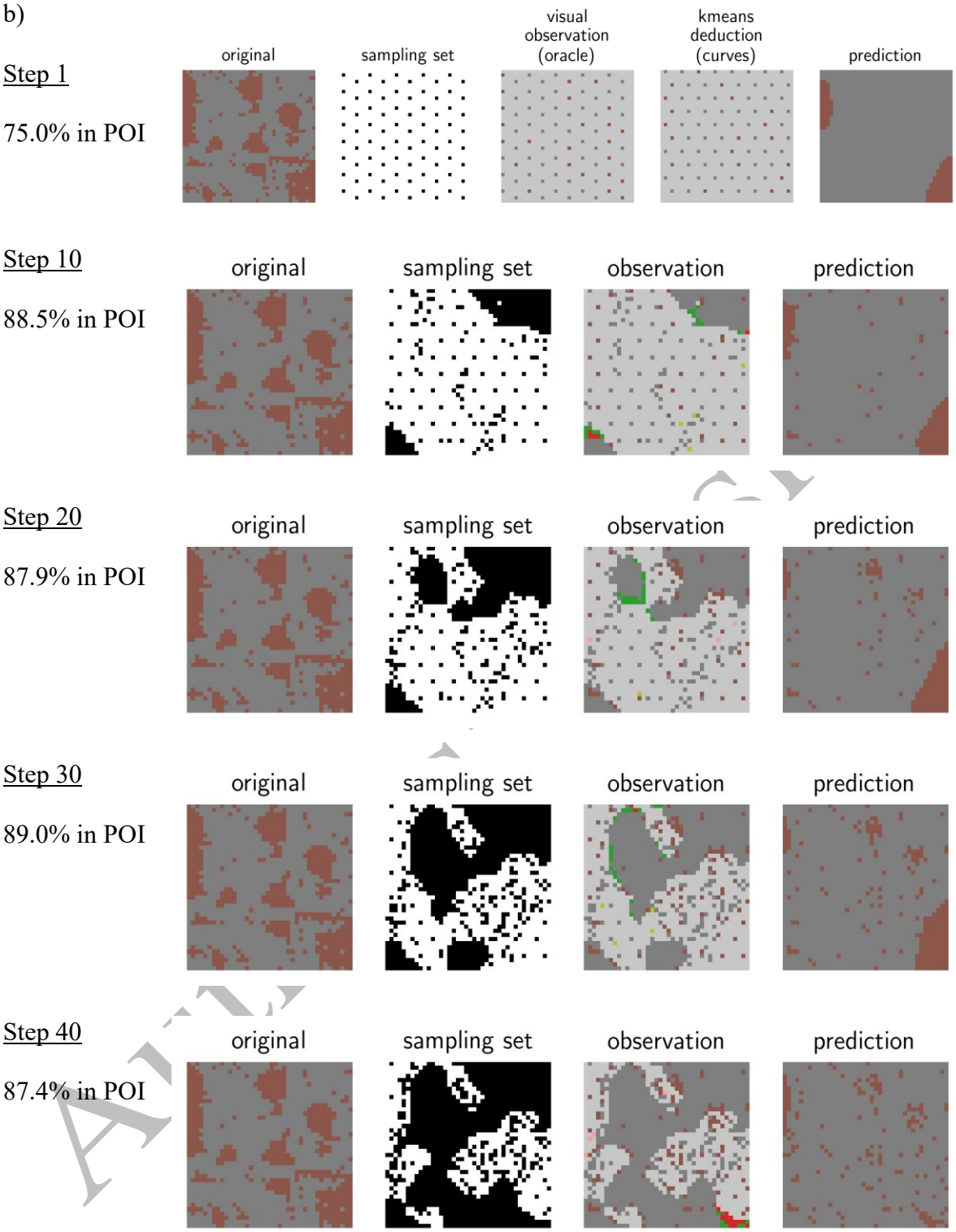
original
sampling set
visual observation (oracle)
kmeans deduction (curves)
prediction
Step 1
75.0% in POI
Step 10
88.5% in POI
original
sampling set
observation
prediction
Step 20
87.9% in POI
original
sampling set
observation
prediction
Step 30
89.0% in POI
original
sampling set
observation
prediction
Step 40
87.4% in POI
original
sampling set
observation
prediction

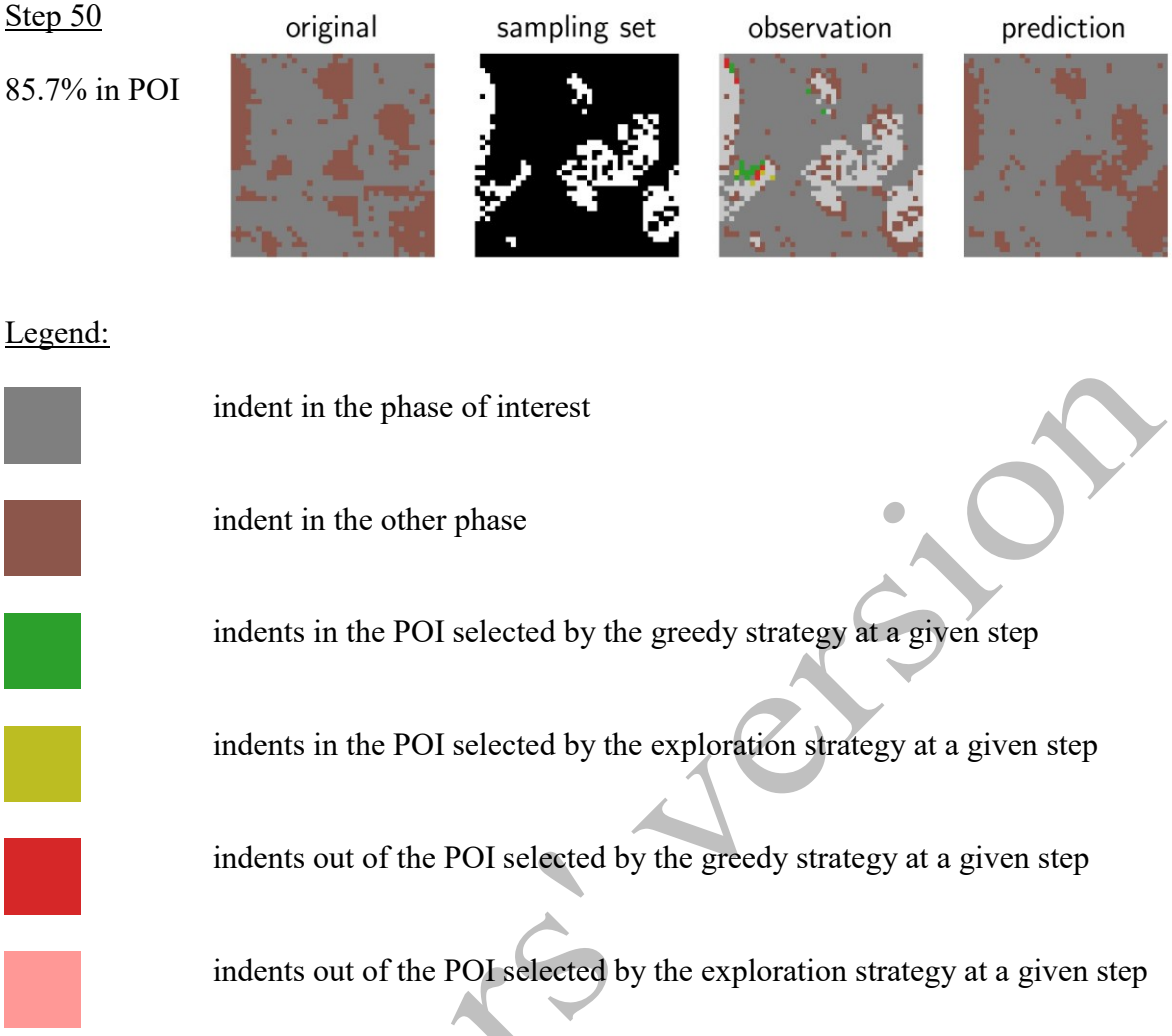

Fig. 12. Maps of the selected indents over time: a) mortar sample, b) cement paste sample. Proportion of indents in the phase of interest (POI) is reported at each step.

In the case of the mortar specimen (Fig. 12 (a)), the initial inference of the GP classifier based on the indentation curves corresponded well with the microscopic observations obtained after the indentation tests. Using the inference, the ε-greedy procedure could find potential positions of the phase of interest within the indented map. Several potential positions of the phase of interest were selected during the first 10 iterations, then some of these zones were extended performing new indents (top right part, middle left part and bottom part), and after 35 steps, most of the largest zones including the phase of interest were found. Therefore, even though the clustering predictions did not coincide with the nature of the indents inferred from

474 microscopic observation, the zones investigated by the algorithm corresponded well with zones
475 with a higher proportion of the phase of interest.
476 In the case of the cement paste specimen, as illustrated in Fig. 12 (b), the number of indents
477 performed in the phase of interest quickly increased. Similar to the case where the microscopic
478 nature of the indents was checked during the algorithm, the algorithm using the indentation
479 curves only correctly advised to perform indents around the clinker particles. This performance
480 could be explained by the distinct mechanical parameters derived from the indentation curves,
481 which can be attributed to the different phases.
482 The algorithm's efficiency has been reported in Fig. 13. In both the mortar and cement paste
483 cases, the proportion of indents located in the phase of interest quickly increased from the value
484 obtained after the initial random Kriging (41% and 70% for mortar and cement paste sample,
485 resp.) to around 58% and 88% for the mortar and cement paste samples, resp. At any step, the
486 proportion of indents in the phase of interest, 56% and 89% on average for the mortar and
487 cement paste resp. (for proportions of tested indents smaller than 45% and 22 to 60% resp.),
488 was higher than the random proportion of the phase of interest in the entire area 42% and 71%
489 for the mortar and the cement paste resp. The drop in efficiency occurring when most indents
490 in the phase of interest have been found was confirmed by the decrease in the proportion of
491 indents in the phase of interest. In the cement paste case, almost all the points in the phase of
492 interest can be found (1055 / 1137) though only 75% of the positions have been tested.
493 Interestingly, as illustrated in Fig. 13, the proportion of indents in the phase of interest, was
494 almost always higher than the random proportion of the phase of interest in the indented area.
495 This observation highlights the performance of the proposed algorithm.

a)

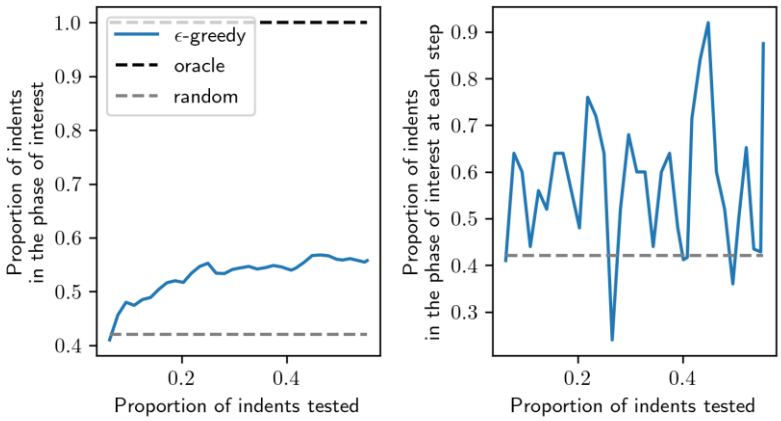

b)

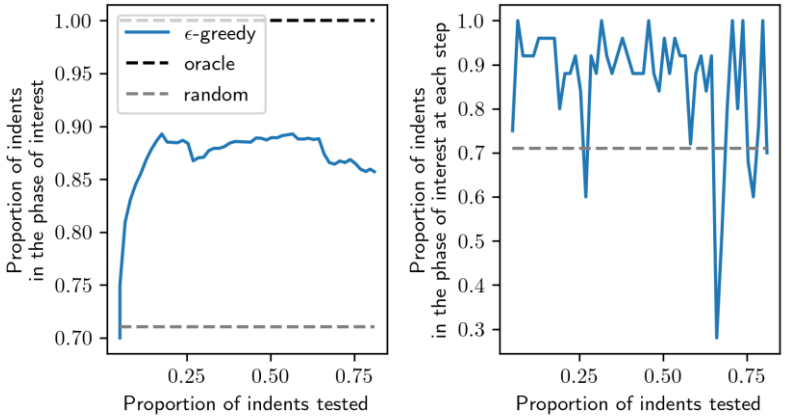

Fig. 13. Evolution of indents in the phase of interest over time using the online algorithm: a) mortar sample, b) cement paste sample.

4. Conclusions

The main objective of the present work was to demonstrate the interest of ε–greedy strategies to automatically select the location of indents to perform during a microindentation or nanoindentation process. Two strategies have been tested: i) an offline algorithm using geometrical information only to infer the next indent location using microscopically identified indents nature and ii) an online algorithm based only on available indentation curves to infer indents nature using unsupervised clustering to feed the ε–greedy algorithm that selects the next

indents to perform. Both algorithms have been tested on cementitious materials, namely, a mortar specimen composed of two major phases, e.g. cement paste and sand, indented with a 500 mN load, and a cement paste specimen composed of hydrates and anhydrous clinker particles indented with a 1 mN load. The main results can be summarized as follows:

- After an initial random Kriging stage giving information about the nature of around 100 indents, ε–greedy strategy led to the selection of indents mostly located in the phase of interest during tens of iterations.
- The proportion of indents in the phase of interest considerably increased with the use of ε–greedy strategies. In the case of the mortar specimen, it increased from 40% to 60% (considering the cement paste as the phase of interest). In the case of the cement paste specimen, the proportion of hydrates within the indents rose from 70% to almost 90%.
- The best parameters associated with the algorithm were found for both samples, and both the exploration strategy and the Gaussian process (GP) classifier kernel's nature can impact the algorithm's efficiency.
- Optimal initial Kriging parameters leading to the best convergence of the algorithm equal to 16, i.e., $1/16^{th}$ of the possible indents are performed initially, provided sufficient information to deconvolve the indentation curves using an unsupervised clustering algorithm.
- The algorithm's efficiency is only slightly affected by using indentation curves only compared to using geometrical information.

Therefore, the proposed method can be successfully applied to select indents in a phase of interest during indentation experiments. By allowing the indentation procedure to be more effective, the proposed approach may open up novel research paths regarding the fast and accurate assessment of the mechanical properties of particular phases of interest in heterogeneous materials during, for example, time-dependant evolutions or after degradation.

Several research paths might be investigated to increase the algorithm performance, like initial knowledge usage (phase proportions) that could help decrease the need for initial Kriging, enhance initial GPC predictions and adapt the stategy to refine the mechanical properties of the phases.

Acknowledgements

The authors would like to thank the Pays de la Loire Region and the European Regional Development Fund (FEDER) for their support.

References

[1] M.J. Mayo, R.W. Siegel, A. Narayanasamy, W.D. Nix, Mechanical properties of nanophase TiO_2 as determined by nanoindentation, J. Mater. Res. 5 (1990) 1073–1082. https://doi.org/10.1557/JMR.1990.1073.

[2] G.M. Pharr, W.C. Oliver, Measurement of Thin Film Mechanical Properties Using Nanoindentation, MRS Bull. 17 (1992) 28–33. https://doi.org/10.1557/S0883769400041634.

[3] A.C. Fischer-Cripps, A simple phenomenological approach to nanoindentation creep, Materials Science and Engineering: A. 385 (2004) 74–82. https://doi.org/10.1016/j.msea.2004.04.070.

[4] Y.-T. Cheng, C.-M. Cheng, Relationships between initial unloading slope, contact depth, and mechanical properties for conical indentation in linear viscoelastic solids, J. Mater. Res. 20 (2005) 1046–1053. https://doi.org/10.1557/JMR.2005.0141.

[5] C.A. Jones, Z.C. Grasley, Short-term creep of cement paste during nanoindentation, Cement and Concrete Composites. 33 (2011) 12–18. https://doi.org/10/dwkkgh.

[6] L. Meng, P. Breitkopf, B. Raghavan, G. Mauvoisin, O. Bartier, X. Hernot, Identification of material properties using indentation test and shape manifold learning approach, Computer Methods in Applied Mechanics and Engineering. 297 (2015) 239–257. https://doi.org/10.1016/j.cma.2015.09.004.

[7] W.C. Oliver, G.M. Pharr, An improved technique for determining hardness and elastic modulus using load and displacement sensing indentation experiments, Journal of Materials Research. 7 (1992) 1564–1583. https://doi.org/10/bdv47f.

[8] P. Trtik, B. Münch, P. Lura, A critical examination of statistical nanoindentation on model materials and hardened cement pastes based on virtual experiments, Cement and Concrete Composites. 31 (2009) 705–714. https://doi.org/10/fd7gb9.

[9] J. Němeček, Creep effects in nanoindentation of hydrated phases of cement pastes, Materials Characterization. 60 (2009) 1028–1034. https://doi.org/10/d6d4q8.

[10] W. Zhu, J.J. Hughes, N. Bicanic, C.J. Pearce, Nanoindentation mapping of mechanical properties of cement paste and natural rocks, Materials Characterization. 58 (2007) 1189–1198. https://doi.org/10/c7znh4.

[11] M. Vandamme, F.-J. Ulm, Nanoindentation investigation of creep properties of calcium silicate hydrates, Cement and Concrete Research. 52 (2013) 38–52. http://dx.doi.org/10.1016/j.cemconres.2013.05.006.

[12] G. Constantinides, K.S. Ravi Chandran, F.-J. Ulm, K.J. Van Vliet, Grid indentation analysis of composite microstructure and mechanics: Principles and validation, Materials Science and Engineering: A. 430 (2006) 189–202. https://doi.org/10.1016/j.msea.2006.05.125.

[13] J. Nohava, P. Haušild, Š. Houdková, R. Enžl, Comparison of Isolated Indentation and Grid Indentation Methods for HVOF Sprayed Cermets, J Therm Spray Tech. 21 (2012) 651–658. https://doi.org/10.1007/s11666-012-9733-6.

[14] F.-J. Ulm, M. Vandamme, C. Bobko, J.A. Ortega, K. Tai, C. Ortiz, Statistical Indentation Techniques for Hydrated Nanocomposites: Concrete, Bone, and Shale, Journal of the American Ceramic Society. 90 (2007) 2677–2692.

[15] B. Vignesh, W.C. Oliver, G.S. Kumar, P.S. Phani, Critical assessment of high speed nanoindentation mapping technique and data deconvolution on thermal barrier coatings, Materials & Design. 181 (2019) 108084. https://doi.org/10.1016/j.matdes.2019.108084.

[16] B. Hilloulin, M. Robira, A. Loukili, Coupling statistical indentation and microscopy to evaluate micromechanical properties of materials: Application to viscoelastic behavior of irradiated mortars, Cement and Concrete Composites. 94 (2018) 153–165. https://doi.org/10.1016/j.cemconcomp.2018.09.008.

[17] Z. Luo, W. Li, Y. Gan, K. Mendu, S.P. Shah, Applying grid nanoindentation and maximum likelihood estimation for N-A-S-H gel in geopolymer paste: Investigation and discussion, Cement and Concrete Research. 135 (2020) 106112. https://doi.org/10.1016/j.cemconres.2020.106112.

[18] G. Constantinides, F.-J. Ulm, The effect of two types of C-S-H on the elasticity of cement-based materials: Results from nanoindentation and micromechanical modeling, Cement and Concrete Research. 34 (2004) 67–80. https://doi.org/10/bxw75c.

[19] L. Sorelli, G. Constantinides, F.-J. Ulm, F. Toutlemonde, The nano-mechanical signature of Ultra High Performance Concrete by statistical nanoindentation techniques, Cement and Concrete Research. 38 (2008) 1447–1456. https://doi.org/10/bjcm88.

[20] J. Fu, S. Kamali-Bernard, F. Bernard, M. Cornen, Comparison of mechanical properties of C-S-H and portlandite between nano-indentation experiments and a modelling approach using various simulation techniques, Composites Part B: Engineering. 151 (2018) 127–138. https://doi.org/10.1016/j.compositesb.2018.05.043.

[21] H. Zhang, Š. Branko, M. Lukovi, E. Schlangen, Experimentally informed micromechanical modelling of cement paste : An approach coupling X-ray computed tomography and statistical nanoindentation, Composites Part B. 157 (2019) 109–122. https://doi.org/10.1016/j.compositesb.2018.08.102.

[22] Y. Gaillard, F. Amiot, Grid nano-indentation as full-field measurements, Composites Part A: Applied Science and Manufacturing. 132 (2020) 105807. https://doi.org/10.1016/j.compositesa.2020.105807.

[23] L. Brown, P.G. Allison, F. Sanchez, Use of nanoindentation phase characterization and homogenization to estimate the elastic modulus of heterogeneously decalcified cement pastes, Materials & Design. 142 (2018) 308–318. https://doi.org/10.1016/j.matdes.2018.01.030.

[24] B. Hilloulin, V.Q. Tran, Using machine learning techniques for predicting autogenous shrinkage of concrete incorporating superabsorbent polymers and supplementary cementitious materials, Journal of Building Engineering. 49 (2022) 104086. https://doi.org/10.1016/j.jobe.2022.104086.

[25] H. Zhang, T. Ji, H. Liu, Performance evolution of the interfacial transition zone (ITZ) in recycled aggregate concrete under external sulfate attacks and dry-wet cycling, Construction and Building Materials. 229 (2019) 116938. https://doi.org/10.1016/j.conbuildmat.2019.116938.

[26] K. Sotiriadis, M. Hlobil, A. Viani, P. Mácová, M. Vopálenský, Physical-chemical-mechanical quantitative assessment of the microstructural evolution in Portland-limestone cement pastes exposed to magnesium sulfate attack at low temperature, Cement and Concrete Research. 149 (2021) 106566. https://doi.org/10.1016/j.cemconres.2021.106566.

[27] H. Chu, T. Wang, L. Han, L. Cao, M.-Z. Guo, Y. Liang, L. Jiang, Vickers hardness distribution and prediction model of cement pastes corroded by sulfate under the coexistence of electric field and chloride, Construction and Building Materials. 309 (2021) 125119. https://doi.org/10.1016/j.conbuildmat.2021.125119.

[28] M. Robira, B. Hilloulin, A. Loukili, G. Potin, X. Bourbon, A. Abdelouas, Multi-scale investigation of the effect of γ irradiations on the mechanical properties of cementitious materials, Construction and Building Materials. 186 (2018) 484–494. https://doi.org/10.1016/J.CONBUILDMAT.2018.07.038.

[29] C. Youssef Namnoum, B. Hilloulin, F. Grondin, A. Loukili, Determination of the origin of the strength regain after self-healing of binary and ternary cementitious materials including slag and metakaolin, Journal of Building Engineering. 41 (2021) 102739. https://doi.org/10.1016/j.jobe.2021.102739.

[30] M. Voltolini, J. Rutqvist, T. Kneafsey, Coupling dynamic in situ X-ray micro-imaging and indentation: A novel approach to evaluate micromechanics applied to oil shale, Fuel. 300 (2021) 120987. https://doi.org/10.1016/j.fuel.2021.120987.

[31] Y. Chang, M. Lin, U. Hangen, S. Richter, C. Haase, W. Bleck, Revealing the relation between microstructural heterogeneities and local mechanical properties of complex-phase steel by correlative electron microscopy and nanoindentation characterization, Materials & Design. 203 (2021) 109620. https://doi.org/10.1016/j.matdes.2021.109620.

[32] K. J. Krakowiak, W. Wilson, S. James, S. Musso, F.-J. Ulm, Inference of the phase-to-mechanical property link via coupled X-ray spectrometry and indentation analysis: Application to cement-based materials, Cement and Concrete Research. 67 (2015) 271–285. https://doi.org/10.1016/j.cemconres.2014.09.001.

[33] W. Wilson, J.M. Rivera-Torres, L. Sorelli, A. Durán-Herrera, A. Tagnit-Hamou, The micromechanical signature of high-volume natural pozzolan concrete by combined statistical nanoindentation and SEM-EDS analyses, Cement and Concrete Research. 91 (2017) 1–12. https://doi.org/10.1016/j.cemconres.2016.10.004.

[34] Y. Wei, X. Gao, S. Liang, A combined SPM/NI/EDS method to quantify properties of inner and outer C-S-H in OPC and slag-blended cement pastes, Cement and Concrete Composites. 85 (2018) 56–66. https://doi.org/10/ghdf8c.

[35] J. Ying, X. Zhang, Z. Jiang, Y. Huang, On Phase Identification of Hardened Cement Pastes by Combined Nanoindentation and Mercury Intrusion Method, Materials. 14 (2021) 3349. https://doi.org/10.3390/ma14123349.

[36] P. Fernandez-Zelaia, V. Roshan Joseph, S.R. Kalidindi, S.N. Melkote, Estimating mechanical properties from spherical indentation using Bayesian approaches, Materials & Design. 147 (2018) 92–105. https://doi.org/10.1016/j.matdes.2018.03.037.

[37] T. Kollar, N. Roy, Trajectory Optimization using Reinforcement Learning for Map Exploration, The International Journal of Robotics Research. 27 (2008) 175–196. https://doi.org/10.1177/0278364907087426.

[38] L. Tai, M. Liu, Towards Cognitive Exploration through Deep Reinforcement Learning for Mobile Robots, ArXiv:1610.01733 [Cs]. (2016). http://arxiv.org/abs/1610.01733 (accessed April 21, 2021).

[39] J. Li, X. Shi, J. Li, X. Zhang, J. Wang, Random curiosity-driven exploration in deep reinforcement learning, Neurocomputing. 418 (2020) 139–147. https://doi.org/10.1016/j.neucom.2020.08.024.

[40] H. Li, Q. Zhang, D. Zhao, Deep Reinforcement Learning based Automatic Exploration for Navigation in Unknown Environment, IEEE Transactions on Neural Networks and Learning Systems. 31 (2020) 2064–2076. https://doi.org/10.1109/TNNLS.2019.292786.

[41] P.-A. Andersen, M. Goodwin, O.-C. Granmo, Towards safe reinforcement-learning in industrial grid-warehousing, Information Sciences. 537 (2020) 467–484. https://doi.org/10.1016/j.ins.2020.06.010.

[42] C.E. Rasmussen, C.K.I. Williams, Gaussian processes for machine learning., MIT Press, 2006.

[43] W. Dabney, G. Ostrovski, A. Barreto, Temporally-Extended {\epsilon}-Greedy Exploration, ArXiv:2006.01782 [Cs, Stat]. (2020). http://arxiv.org/abs/2006.01782 (accessed February 10, 2022).

[44] T. Liu, X. Li, L. Tan, S. Song, A novel adaptive greedy strategy based on Gaussian mixture clustering for multiobjective optimization, Swarm and Evolutionary Computation. 61 (2021) 100815. https://doi.org/10.1016/j.swevo.2020.100815.

683 [45] M. Vandamme, F.-J. Ulm, P. Fonollosa, Nanogranular packing of {C-S-H} at
684 substochiometric conditions, Cement and Concrete Research. 40 (2010) 14–26.
685 http://dx.doi.org/10.1016/j.cemconres.2009.09.017.

686